ACS APPLIED MATERIALS & INTERFACES

RESEARCH ARTICLE

www.acsami.org

All Electrochemical Fabrication of a Platinized Nanoporous Au Thin-Film Catalyst

Daniel A. McCurry, Martha Kamundi, Matthew Fayette, Fred Wafula, and Nikolay Dimitrov*

Department of Chemistry, SUNY at Binghamton, P.O. Box 6000, Binghamton, New York 13902-6000, United States

ABSTRACT:

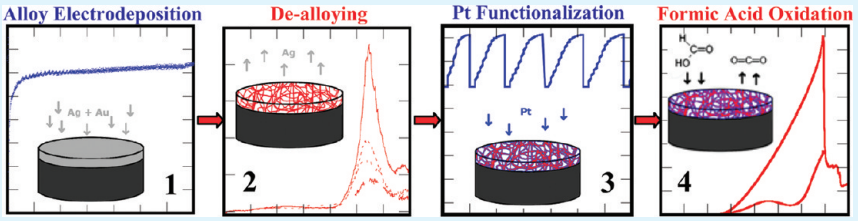

In an effort to decrease the high cost associated with the design, testing, and production of electrocatalysts, a completely electrochemical scheme has been developed to deposit and platinize a nanoporous Au (NPG) based catalyst for formic acid oxidation. The proposed route enables synthesis of an alternative to the most established, nanoparticles based catalysts and addresses issues of the latter associated with either contamination inherent from the synthetic route or poor adhesion to the supporting electrode. The synthetic protocol includes as a first step, electrochemical codeposition of a $Au_{(1-x)}Ag_x$ alloy in a thiosulfate based electrolyte followed by selective electrochemical dissolution (dealloying) of Ag as the less noble metal, that generates an ultrathin and preferably continuous porous structure featuring thickness of less than 20 nm. NPG is then functionalized with Pt (no thicker than 1 nm) by surface limited redox replacement (SLRR) of underpotentially deposited Pb layer to form Pt-NPG. SLRR ensures complete coverage of the surface with Pt, believed to spread evenly over the NPG matrix. Testing of the catalyst at a proof-of-concept level demonstrates its high catalytic activity toward formic acid oxidation. Current densities of 40−50 mA cm^{-2} and mass activities of 1−3 A.mg^{-1} (of combined Pt−Au catalyst) have been observed and the Pt-NPG thin films have lasted over 2600 cycles in standard formic acid oxidation testing.

KEYWORDS: Pt, nanoporous Au, dealloying, platinization, catalysis, formic acid oxidation

INTRODUCTION

The drive toward efficient and durable fuel cells is founded on the development, characterization, and testing of a variety of catalysts that one way or another include Pt. To minimize the cost, most of the catalysts have been synthesized in the form of nanoparticles. Nanoparticles are superior to other type of materials applicable in catalysis with their large surface area to volume ratio and unique physical and chemical properties.[1] In the process of catalyst development, the nanoparticles are either brought in contact with a carrier electrode (for instance glassy carbon, GC) mechanically or been grown in the synthetic bath directly on a support which helps to relieve some of the problems introduced by the capping agents or associated with aggregation.[2] Thus, the nanoparticles interact with the substrate either directly or through the capping agent molecules; generally through physisorption. The nanoparticle adsorbates are therefore very fragile and effects associated with either incomplete removal of the capping agent or with mechanical disconnection and/or aggregation of particles often lead to a rapid reduction of the electrochemically active surface area (ECASA).[3,4] Nafion is occasionally used to help prevent the loss of nanoparticles from the surface, but this introduces another material that may block catalytically active sites and effectively reduce ECASA.[5]

An electrodeposition approach for synthesizing the catalytically active layer directly on an electrode would not only provide for better adhesion compared to the nanoparticle route (the charge transfer takes place on the electrode surface) but would also enable a complete control over the amount of the deposit, thus reducing the overall synthetic cost. If the electrodeposited layer is a binary alloy with controlled thickness and elemental composition, a nanoporous catalyst with tunable pore and ligament size could be generated by selective electrochemical dissolution (dealloying) of the less noble metal.[6] In ideal life, the result of these sequential electrochemical steps would lead to the development of a continuous layer representing a much more resilient catalyst that because of the lack of capping agent would ensure better electron transfer between the substrate and the deposit.[7]

Forming such alloys on foreign substrate surfaces in research practice has traditionally involved methods such as chemical vapor deposition and sputtering techniques to co-deposit the metals or depositing one layer of metal at a time followed by thermal annealing to mix the metal layers.[7−11] The method discussed in the present study provides a cost-effective alternative

Received: August 23, 2011
Accepted: October 7, 2011
Published: October 07, 2011

dx.doi.org/10.1021/am2011433 | ACS Appl. Mater. Interfaces 2011, 3, 4459–4468

Scheme 1. Key Steps of the Pt-NPG Thin-Film Fabrication

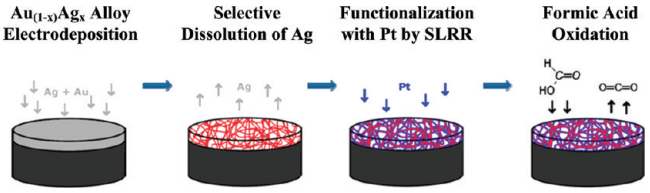

represented by electrochemical codeposition of both alloy constituents. Once electrodeposited as a thin film, the alloy is subjected to dealloying that not only serves to generate a porous structure with highly developed surface area,[6] but also provides fine-tuning mechanisms for control over the amount of less noble metal retained in the structure.[12]

The electrodeposited alloy could be Pt-based, but cost-effectiveness and the tendency of electrochemically generated Pt (or Pt-alloy) films to grow preferentially in 3D mode[13,14] warrants electrodeposition of Au-based alloys instead. It needs to be noted that Au is not considered as attractive catalyst,[15] and yet, much research has shown that at the nanoscale level, a tiny amount of Pt could substantially enhance the catalytic ability of Au.[7,10,15−17] Using surface limited redox replacement (SLRR),[18] the Au could be coated with one or a few layers of Pt by galvanically displacing underpotentially deposited (UPD) Cu[19] or Pb[20] monolayers. SLRR has the advantage of coating the entire surface because it relies on the displacement of a (perfectly conformal with the substrate) UPD sacrificial layer by the metal of interest.[21] It has been also shown that a small amount of Pt is able to make a Au surface behave as if it was pure Pt due to synergistic effects.[19] Recently, nanoporous Au structures coated by Pt (Pt-NPG) using different electrochemical approaches have been studied extensively in the literature and demonstrate very high catalytic activity and durability.[17,22−24] The reduced amount of Pt also results in a catalyst more resistant to CO poisoning, so a much more robust catalyst is expected for the as-prepared surface.[3]

The all-electrochemical method proposed in this work for preparing and examining the Pt-NPG thin films is outlined in the Scheme 1 presented below. The Ag−Au alloy is first electrodeposited in a cell whereby the amount of Ag and Au in the deposit is believed to be controlled by the molar ratio of those metals in a joint thiosulfate based solution. Dissolution of the Ag is then performed in another cell in order to develop nanoporosity within the deposit. As previously described, SLRR is used to functionalize the NPG surface to make it catalytically active toward formic acid oxidation.

More specifically, this study includes a formation of Pt-NPG thin film on two substrates, Au and GC. The current densities for formic acid oxidation on each were similar initially, but the thin film deposited on Au was continuous and smooth while the deposit on GC was comprised of partially overlapping spherical alloy particles with density that was strictly nucleation dependent. Further optimization of the conditions and parameters used in this study may very well lead to a robust catalyst suitable for practical applications, especially because of the minimal amount of Pt required to produce such a catalyst.

EXPERIMENTAL SECTION

The following chemicals were used for the experiments: H_3PO_4 (GFS Chemicals 99.999%, 85% solution), ethylene glycol (Fischer Scientific, Certified), $Na_2S_2O_3.5H_2O$ (Alfa Aesar 99+%), AuCl (Aldrich 99.9% metals basis), $AgClO_4 \cdot H_2O$ (Aldrich 99.999%), $NaClO_4 \cdot H_2O$ (Aldrich 99.99% metals basis), $Pb(ClO_4)_2H_2O$ (Aldrich ≥99.995%), $HClO_4$ (GFS Chemicals 70%, veritas redistilled), $KPtCl_4$ (GFS Chemicals, 98%), HCOOH (JT Baker 88%), HNO_3 (Fischer Scientific, Certified ACS Plus), and ethanol (Pharmco-AAPER, 200 proof ACS/USP grade). All solutions were prepared with the chemicals as received by the vendors and Barnstead Nanopure water ($R \geq 18.2$ MΩ cm^{-1}).

Table 1. Molar Ratios of Ag^+ and Au^+ Cations in Solution

solution molar ratio (Ag:Au)	Ag^+ (mM)	Au^+ (mM)
1:1	0.40	0.40
3:2	0.55	0.36
2:1	0.60	0.30

Electrode Preparation. Polycrystalline cylindrical Au (99.99%) working electrodes (diameter 6 mm) were mechanically polished down to 1 μm with alumina powder on a Buehler polishing pad. Then the Au electrodes were sonicated in water for five minutes and rinsed with deionized (DI) water. Before use, the Au samples were submerged in concentrated HNO_3 at 50 °C and rinsed again with Barnstead Nanopure water.

Cylindrical GC working electrodes (Goodfellow) (diameter 5 mm) were mechanically polished down to 1 μm with alumina powder followed by 0.05 μm diamond suspension on Buehler polishing pads. Between the alumina and diamond polishing, the electrode was sonicated for five minutes in a solution containing ethanol and Barnstead Nanopure water.

Cylindrical Cu working electrodes (diameter 6 mm) were mechanically polished down to 1200 silicon carbide paper followed by 0.5 μm alumina powder on a Buehler polishing pad. The electrode was then electrochemically polished in a 5:3:2 phosphoric acid:glycol:water solution at 3.84 V with a Pt ring serving as counter electrode.

The Pt wire used as counter electrode in all experiments was pretreated by etching in 50% HNO_3 at 50 °C before being flame annealed. The Ag wire used as pseudoreference electrode in the deposition and dealloying runs was also etched in 50% HNO_3 at 50 °C but was not flame annealed to prevent oxidation of the surface. Mercury mercurous sulfate electrode (SSE) was used as reference electrode in the SLRR and formic acid oxidation experiments.

$Au_{(1-x)}Ag_x$ bulk alloy strips were polished with a cotton applicator using 1 μm alumina powder and water. Areas that were to be excluded from dealloying were coated with nail polish.

Thin-Film Alloy Deposition. $Au_{(1-x)}Ag_x$ thin film alloys were electrochemically deposited using a Princeton Applied Research Model 173 Potentiostat/Galvanostat with a model 276 Interface and model 270/250 Research Electrochemistry Software 4.00 from solutions containing Ag−Au molar ratios of 1:1, 3:2, and 2:1 in 0.1 M $Na_2S_2O_3$ on Au and GC working electrodes. Concentrations are listed in Table 1. Au(I)Cl complex provided the source of Au^+ cations and $AgClO_4$ provided the source of Ag^+ cations. All solutions were used within a week of preparation to prevent effects associated with spontaneous metal reduction. Different potentials were applied depending upon the substrate used. On Au, the deposition potential was −0.150 V and on GC, the deposition potential was −0.260 V. The thickness of the deposit was controlled by the duration of the applied potential. Samples were rinsed thoroughly with Barnstead Nanopure water. An additional deposit of each ratio was performed on Cu at −0.500 V for 6 h to obtain a very thick deposit. These samples were used for energy dispersive X-ray spectroscopy (EDX) in order to determine the exact ratio of Ag−Au in the deposit. SEM/EDX measurements were performed using a FEG-SEM Supra 55VP.

Pb UPD for surface area measurements[25] was performed in a solution of 0.1 M $NaClO_4$ and 3 mM $Pb(ClO_4)_2$ with a pH of 2 adjusted with

$HClO_4$. The potential was scanned from 0.600 to 0.010 V for 4 cycles at 20, 10, and 5 mV s^{-1} versus Pb/Pb^{2+} pseudo reference electrode with a platinum wire counter electrode using a Pine bipotentiostat model AFCBP1 with PineChem 2.8.0H software. The solution was purged with ultrahigh purity nitrogen for 2 h prior to Pb UPD and had N_2 passed over the surface of the solution during the scans. Charge was integrated from the curve and was recorded as the average of the forward and reverse scans.

Dealloying. The silver was removed from the deposited alloy using 0.5 mM $AgClO_4$ in 50 mM $HClO_4$ with the potentiostat used for deposition. For determination of the critical potential, the applied potential was scanned from 0 to 0.800 V at a sweep rate of 0.3 mV s^{-1} versus Ag/Ag^+ pseudo reference electrode. For samples used for SLRR, stripping analysis was performed by chronoamperometry with a constant potential 0.100 V more positive than the critical potential for that ratio instead of linear sweep voltammetry until the nominal current decreased to zero. Samples were rinsed clean with Barnstead Nanopure water. $Au_{(1-x)}Ag_x$ bulk alloy strips of known composition were also dealloyed using the linear sweep voltammetry parameters as described above to serve as a comparison of the critical potential behavior. The samples were thoroughly rinsed with Barnstead Nanopure water and SEM was used to examine the morphology of the dealloyed surfaces.

Pb UPD for surface area measurements was again performed on the surface of the electrode using the same procedure as outlined in the Thin-Film Alloy Deposition section. The average integrated charge was recorded and used to determine the factor of surface area increase by comparing to the integrated charge from the initial deposit of the alloy.

Pt Functionalization. Five replacements of Pb UPD layer by Pt(II)Cl complex[20] using surface-limited redox replacement with an OMNI 90 (Cypress Systems) potentiostat coupled to a Cypress Systems coupling electronics module and National Instruments Analog-to-Digital converting board were performed on the dealloyed Au and GC samples in a solution containing 0.1 M $NaClO_4$, 1 mM $HClO_4$, 1 mM $Pb(ClO_4)_2$, and 0.5 mM $KPtCl_4$ and recorded using Dasylab 9.00 software, following a protocol recently developed by our group.[20] A 1 s pulse at −0.830 V vs SSE was applied to allow percolation of the Pb throughout the nanoporous structure. After, the applied potential was released and the potential was monitored until it reached +0.050 V. At this high limit, the pulse was reapplied and the cycle resumed for each replacement.

H UPD was performed on the surface of the functionalized electrode from +0.400 to −0.680 V at 50 mV s^{-1} vs SSE in a 0.5 M H_2SO_4 solution. The solution was purged with nitrogen for 2 h prior to H UPD and had N_2 gas passed over the surface of the solution during the analysis. The charge was calculated by running chronoamperometry at −0.690 V for the negative scan and at −0.400 V for the positive scan, then averaging the integration of both curves.

Formic Acid Oxidation. Prior to formic acid oxidation, the samples were electrochemically annealed by rapidly scanning (300 mV s^{-1}) between −0.740 and +0.450 V in the H UPD solution for 50 cycles to activate the surface. The testing followed a procedure developed and described in our earlier work.[26] More specifically, formic acid oxidation was performed on the Pt-NPG surface in 2 M HCOOH and 0.1 M $HClO_4$ from −0.510 to +0.800 V vs SSE repetitively until the current density decayed to about zero. After a certain number of cycles, the working electrode was removed from the formic acid cell and checked with H UPD to ensure that the surface was still intact and to measure the ECASA.

RESULTS AND DISCUSSION

1. Thin-Film Alloy Deposition. Baths for Au electrodeposition containing sulfite or thiosulfate are common alternatives to industrially used cyanide baths. Such baths have been studied extensively due to the high quality of the generated deposits and owing to their relative environmental benignity.[27−31] In this work we used a thiosulfate based bath for depositing $Au_{(1-x)}Ag_x$ alloys, taking advantage of the solubility of Ag^+ cations and Au(I)Cl complex in that environment. Furthermore, because both cations in solution feature practically identical size (0.4% difference) and charge (+1), it was expected that each would deposit at a similar rate and the molar ratio of cation concentrations in solution would be equal to the ratio of Ag and Au in the deposit. While a bulk deposition process is usually carried out at substantially higher concentration of the electroactive species, the concentrations in our work presented in Table 1 were limited by the stability of Au(I)Cl in $Na_2S_2O_3$ solution. Indeed, as also mentioned elsewhere, a small amount of S precipitate was immediately formed upon addition of Au(I)Cl to a 0.1 M $Na_2S_2O_3$ solution.[28,31,32]

The potential of −0.150 V versus Ag/Ag^+ pseudo reference electrode was used for deposition on Au substrate since in separate polarization curves for both solutions it was found to be sufficiently negative for the mass transport controlled reduction of both Ag^+ and Au^+ cations. A very shiny deposit with a silver looking color was obtained in agreement with expectations of a continuous and flat layer grown on the surface. The current density reached a steady state which allowed for certain thicknesses to be deposited depending upon the time of deposition, as shown in Figure 1a. Overall, the current density was occasionally affected by the age of the solution or the morphology of the polished surface and was not strictly dependent upon the ratio of Ag and Au present in solution. An applied potential of −0.150 V with a GC electrode practically did not produce any visible deposit, however, likely due to high over potential of GC associated with a hindered catalytic activity. Instead, GC required a more negative potential (at least −0.260 V) than the Au substrate in order to deposit the alloy. Because of the lower overpotential needed, the deposition on GC occurred at a slightly lower current density for all compositions when compared to deposition on Au. Also, the current was noted to decrease steadily from its initial value rather than decreasing to a steady state as illustrated in Figure 1b. Whereas Au assumed similar activity throughout the deposition, GC began as a relatively passive substrate that was gradually activating due to the formation of a metal surface over the course of the experiment. As a result, the active surface area was increasing owing to the steady growth of the metal clusters nucleated initially on the GC. EDX analysis of the thin film $Au_{(1-x)}Ag_x$ alloys, specifically deposited on Cu for this analysis from the solutions summarized in Table 1 indicated 77:23, 74:26, and 70:30 Ag:Au for the 2:1, 3:2, and 1:1 solution compositions, respectively. No traces of S were present in the deposits, indicating that there was no contamination originating from the thiosulfate solution during the deposition. Although it was expected that the Ag and Au would deposit in the ratio in which they were present in solution, EDX analysis revealed that Ag had a much higher atomic percentage than expected. One reason for this disparity in Ag−Au ratios might be the relative stabilities of the Au and Ag thiosulfate complexes. Au (I) thiosulfate has a larger stability constant, $\beta_{Au} = 1.3 \times 10^{26}$, than Ag (I) thiosulfate, $\beta_{Ag} = 4.2 \times 10^{13}$, so it was much easier for Ag^+ to leave the complex and reduce on the surface of the electrode compared to the Au^+ cation.[31,33]

2. Dealloying. *2.1. Electrochemistry and Structural Evolution.* The simplest dealloying route for $Au_{(1-x)}Ag_x$ alloys involved immersing the samples in a nitric acid bath and allowing the Ag to

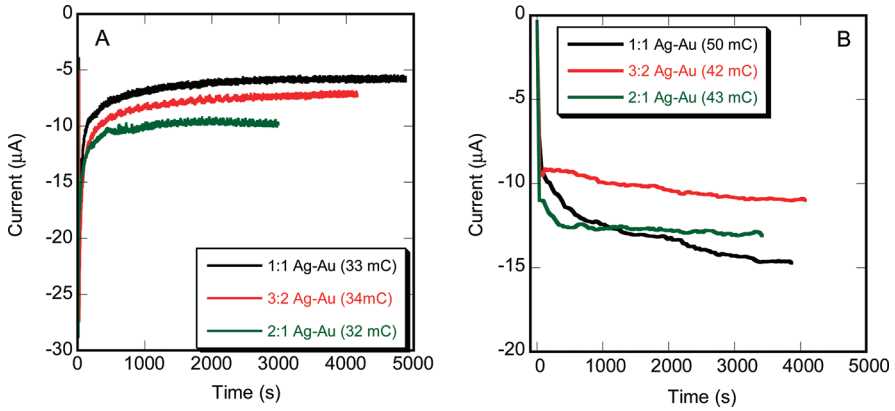

Figure 1. Chronoamperograms showing the alloy deposition at (A) −0.150 V vs Ag/Ag^+ on 6 mm Au and (B) −0.260 V vs Ag/Ag^+ on 5 mm GC. Total deposition charge presented in the legends.

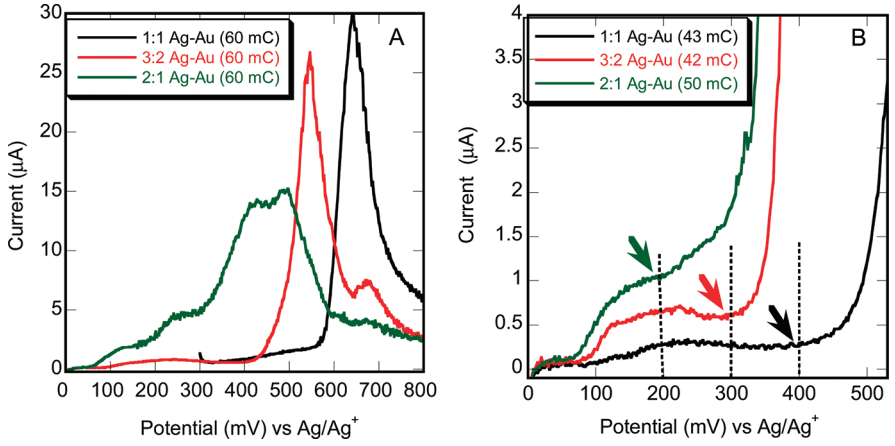

Figure 2. Anodic polarization curves showing dealloying of $Au_{(1-x)}Ag_x$ samples on (A) Au and (B) GC at sweep rate of 0.3 mV s^{-1}. Total deposition charge presented in the legends.

dissolve over time.[4,9,11,17] Such a method affords little control over the dissolution process. For this reason, the Ag selective dissolution in the present study was performed electrochemically following a well established dealloying protocol.[12,34] A large increase in current was not visible until the dealloying critical potential,[34] (E_c) was reached for each alloy during linear sweep voltammetry. Figure 2a illustrates the anodic curve for the removal of Ag from the alloy deposited on Au substrate. Each composition appeared to have slight dissolution prior to the critical potential, but the 2:1 Ag:Au composition displayed the most pronounced, multistep precritical potential dissolution behavior. It needs to be noted that unlike their bulk counterparts,[34] the dealloying curves in this work feature peak structures positive to E_c (Figure 2a). The specific curve shape however is simply due to the limited amount of Ag in the alloy. Once all the Ag is selectively dissolved, the rate of the process starts rapidly decreasing toward a complete hold thereby generating the peak structure in the Figure 2 anodic curves.

The dealloying of the samples was carried out until complete removal of the Ag was achieved (as measured by the current running through the system). In general, no substantial Ag retention within the nanostructure was expected during the dealloying as the relatively low pH, is not favorable for Ag retention[12] and the very low thickness of the dealloyed layers would not allow for a massive restructuring during which Ag trapping mainly occurs.[12] With all of the above said, any possibly retained Ag was not expected to have a negative influence on the catalytic properties of the NPG, because it has been reported that there may be synergistic benefits to incorporating Ag into the catalyst.[11,15] It was also not expected that any Au was dissolved and then reduced back on to the surface because this would lead to a greater number of nucleation sites and the clusters visible in Figure 3d and e would not be so isolated.[35,36]

The massive removal of Ag in the course of dealloying leads to an increased amount of stress in the system. This stress caused significant cracking on the deposits on Au as shown in Figure 3c and d.[36,37] Cracking was not observed on the GC deposits most likely because they did not feature a continuous surface and therefore did not develop a significant amount of stress as the structural imbalance generated during dealloying was accommodated by the spherical alloy particles (Figure 3e and f).

Overall the critical potentials for the alloy deposits on the Au substrates followed the trends typical for their bulk counterparts and represented by more positive E_c with the increase in Au content. Interestingly enough, the E_c values in this work turned to be nearly equal to those of bulk alloys after considering the composition determined by EDX. The very close match in the E_c values indicated that the mechanism for dealloying of thin films

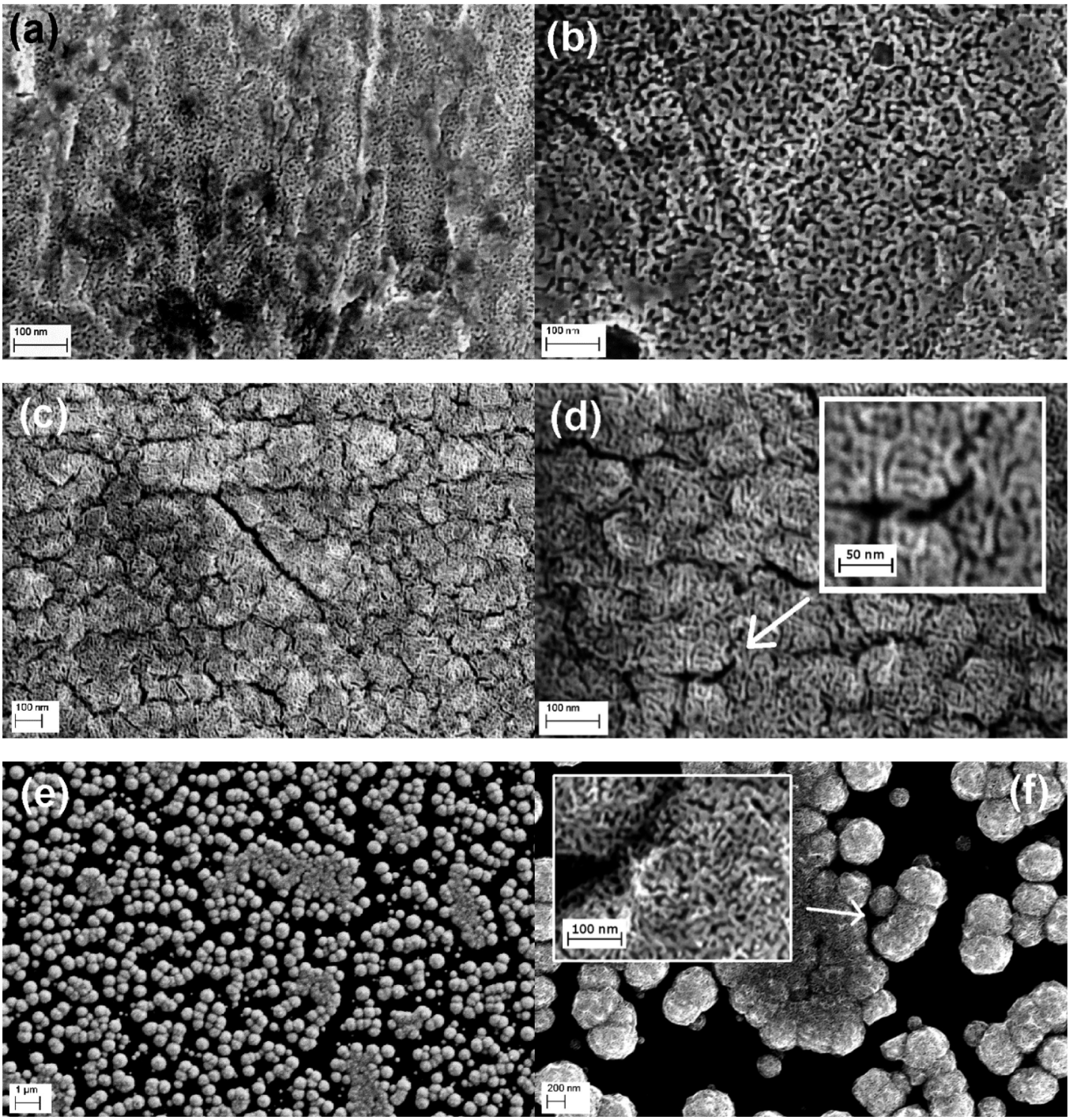

Figure 3. SEM images of dealloyed (a) bulk 70:30 Ag:Au, (b) bulk 80:20 Ag:Au, (c) 3:2 Ag:Au on Au, (d) magnified 3:2 Ag:Au on Au, (e) 3:2 Ag:Au on GC, and (f) magnified 3:2 Ag:Au on GC.

and bulk samples is generally the same. It needs to be noted that in this study the critical potentials were determined by observing the potential range where the sharp increase in current began for each dealloying run. Although this way was less accurate than the one proposed by A. Dursun et al.,[38,39] it was sufficient for the purposes of the present study admitting that no steady state current measurements could be made on samples thinner than 100 nm.[34]

It was also observed that the critical potentials on GC alloy deposits were consistently less by about 0.1 V, as shown in Figure 2. For comparison, critical potentials for all of the samples deposited on Au and GC as well as the bulk $Au_{(1-x)}Ag_x$ alloy samples are summarized in Table 2. Also, SEM images of the dealloyed surfaces in Figure 3 show that the bulk strips and the thin alloy deposits on Au feature flat and continuous surfaces, whereas the nanoporous structures present on GC are separated into clusters.[40] Taking into account all facts, the negative shift in E_c could be attributed to the curved surface of the spherical clusters, grown on the GC surface unlike the continuous layers deposited on the Au substrates.

Apparently, regardless of the shape differences, after dealloying all three type of samples feature the characteristic for NPG substrates: two-phase, interpenetrating solid-void morphology.[41] It is interesting that in spite of the spherical cluster shape, the critical potential behavior persisted in the dealloying of all $Au_{(1-x)}Ag_x$ layers deposited on GC. As a result, as seen in Figure 3f, the nanoporous structure expected after dissolution is largely present within the dealloyed clusters on GC. It is important to note, however, that the 2:1 dissolution curves show multiple dissolution steps prior to E_c, which makes it difficult to identify clearly the critical potential in certain cases. These steps may be caused by the low content of randomly distributed Au atoms in the alloy deposit with this composition. This in turn results in lack of a Au percolation backbone that would otherwise uniformly impact the selective Ag dissolution. This automatically leads to uneven distribution of the surface passivity manifested by the quazi-critical potential behavior seen in Figure 2B.

2.2. Surface Area Measurements. The more common Brunauer, Emmett and Teller (BET) method of determining surface area of porous structures was not considered viable in our work because of (i) the extremely small size of the samples used and (ii) the elevated temperature at which BET must be performed that would promote NPG structure coarsening.[25,42] Instead, the electrochemical analog of BET[25] was used for measuring the ECASA of NPG. In this approach, the charge measured through either formation or stripping of the Pb UPD monolayer is normalized by the charge density that the same Pb UPD layer features on flat polycrystalline Au surface, 320 μC cm^{-2},[25] to give the developed NPG surface area.

Table 2. Critical Potentials for Each Sample

substrate	composition (Ag:Au)	Critical Potential, E_c (V)
Au	1:1 (70:30)	0.560
	3:2 (74:26)	0.420
	2:1 (77:23)	0.310
GC	1:1 (70:30)	0.400
	3:2 (74:26)	0.300
	2:1 (77:23)	0.200
bulk[a]	70:30	0.560−0.580[25,34]
	80:20	0.400−0.420[25,34]

[a] Bulk strips dealloyed in this work feature identical critical potential behavior.

The Pb UPD curves presented in Figure 4 do not show many of the characteristic peaks associated with Pb UPD on Au prior to dealloying possibly because of the inclusion of Ag in the surface. Once dealloyed, the Au (111) peak at 0.200 V and the (100) and (110) peaks at 0.450 V versus Pb/Pb^{2+} pseudoreference electrode are visible. The peaks are broad, because of the slower diffusion of the Pb through the NPG network that normally warrants work at lower sweep rate.[25] In this study, however, the alloy thickness was generally low, so no changes were observed on the curves at scan rates of 10 and 5 mV s^{-1}.

Table 3 shows the surface area measured using Pb UPD on alloy deposits of varying ratios separately on Au and GC substrates. Only a small charge was calculated by integration of the CV curves on the as-deposited alloy surface. As surface area developed during dealloying, the amount of Pb underpotentially depositing on to the surface greatly increased. Increases in surface area of over six times were observed for alloy deposits on Au. The initial surface area calculated on GC was less than that on Au because of the smaller size of the GC electrode (0.20 cm^2 versus 0.28 cm^2 for Au) and also relatively limited surface coverage of the alloy deposited on GC. Calculated surface areas were slightly larger than expected on the alloy surfaces likely due to clusterlike shape of the deposit not allowing for full surface coverage.

The surface area developed by dealloying could be compared with the theoretical surface area derived from a set of separated nanoparticles (for the sake of simplicity nanocubes) that represents the mass equivalent of the Au in the NPG layer. The size of these nanocubes would be equal to the porosity length scale of NPG.[25] One could take for an estimate the 3:2 Ag:Au alloy which

Table 3. Surface Area Measurements for Alloys on Au and GC Substrates before and after De-Alloying

		surface area (cm^2)		
substrate	ratio (Ag:Au)	before	after	roughness factor
Au	1:1 (70:30)	0.41	2.65	6.46
	3:2 (74:26)	0.38	2.37	6.24
	2:1 (77:23)	0.40	2.35	5.88
GC	1:1 (70:30)	0.18	0.86	4.78
	3:2 (74:26)	0.34	1.65	4.85
	2:1 (77:23)	0.22	0.92	4.18

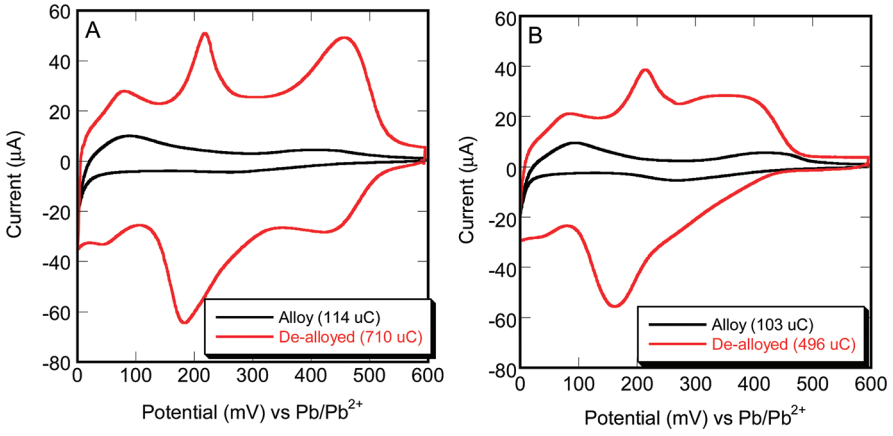

Figure 4. CV curves showing Pb UPD at 20 mV s^{-1} before and after dealloying carried out on 3:2 Ag:Au deposited (A) on Au (11.1 mC Ag stripping charge upon dealloying) and (B) on GC (9.9 mC Ag stripping charge upon dealloying). Sweep rate −20 mV.s^{-1}.

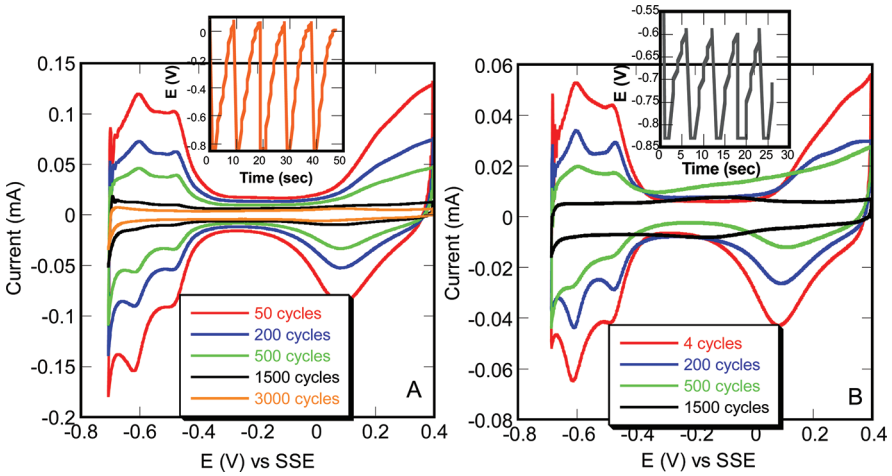

Figure 5. CV curves showing H UPD on Pt-NPG from 1:1 Ag:Au deposit on (A) Au substrate and (B) GC substrate after different number of cycles in formic acid oxidation testing. Sweep rate −50 mV s^{-1} Insets: Potential transients depicting the Pt coating carried out by SLRR.

after dealloying is most likely (conservatively) about 15−20 nm thick (see the dealloying curve in Figure 2b and the stripping charge originating from Ag only) and features a porosity length scale of 8−10 nm (see the SEM images in Figure 3). Then, taking the amount of Au atoms in a cylinder featuring base with area of 1 cm^2 and height of 20 nm and distributing this amount in nanocubes with five exposed sides (one of the sides would be blocked by the substrate or another particle) with edge of 8 nm, one could easily calculate that the maximum (theoretical) ECASA for that sample to be 9−13 cm^2. The range of surface area increase of 4−7 cm^2 (normalized per 1 cm^2 flat surface) registered in this work appears to be a reasonable match of the real surface area to the theoretical one. Furthermore, similar estimates carried out for nanoparticle catalysts never yield a surface area matching the theoretical one, mostly because of contaminations, particle overlapping and/or aggregation.[1] It is very likely that usage of thinner samples in our future work could narrow the gap between theoretical and experimental values. Thus far, work in that direction was out of the immediate scope of this proof-of-concept activity.

3. Pt Functionalization. To activate the NPG surface and enable its suitability for organic fuel catalysis (in this work formic acid oxidation) and to counteract the coarsening of the catalyst, the as-dealloyed layers were coated with several monolayers of Pt, using SLRR of Pb UPD layer by Pt(II) complex. This approach was recently proposed by our group[20] as alternative to platinization done by SLRR of Cu UPD,[10] which is prone to low yields as well as surface roughening upon multiple replacement events. The key advantage of the Pb UPD-assisted protocol is the higher efficiency of each SLRR step allowing for near-complete coverage of the NPG surface and no noticeable increase in surface area up to 10 replacement events.[20] This is the first application of the Pb UPD-assisted platinization approach for coating of a real catalyst (the previous work was performed only on flat Au surfaces[20]).

Five replacements of Pb by Pt were performed in order to generate a Pt thin film. Potential transients for these replacements are shown in the insets of Figure 5. According to that protocol, the Pt coating would have an equivalent thickness to 2−3 monolayers. After the applied potential was removed, the system was allowed to go to open circuit potential (OCP), during which Pt displaced galvanically the Pb. It should be noted that the replacement events on NPG took approximately twice as long to occur as compared to flat Au.[20] This decrease in replacement rate was most likely due to the hindered mobility of Pt throughout the nanosized pores present in the structure. After Pt was grown it was possible to perform ECASA measurements by H UPD on the Pt/NPG surface and taking into account that a layer of adsorbed H on flat Pt(111) carries charge density of 210 $\mu C\ cm^{-2}$.[43] The surface area of Au still uncovered by Pt and the GC underneath would be rendered inactive, as hydrogen will only UPD on Pt. Ideally, the surface area of the grown Pt would be equal to the surface area of Au measured by Pb UPD since it was expected that the entire NPG surface was covered with Pt. Also, roughening due to the addition of Pt was not considered to be significant since (as mentioned earlier) no roughness evolution has been registered for up to 10 SLRR grown Pt monolayers, corresponding to about 3 nm thickness.[20] Because the replacement by Pt required more time than on a flat surface, however, it was possible that side reactions had more impact during the displacement thereby lowering the efficiency and eventually reducing the overall surface area measured by H UPD. The CV curves in Figure 5 showed characteristic peaks of H UPD formation and stripping on Pt in the −0.670 to −0.400 V region. Other peaks present higher than −0.400 V corresponded to oxide formation/stripping on the surface and were not considered in surface area calculations.

Overall, the surface area of Pt was found to be practically identical or just slightly less than the surface area of NPG. This is expected even upon imperfections of the Pt coating as many prior studies concerning Pt/NPG samples reasoned that synergistic effects arising from the electronic modification of Au and Pt and the mechanism of Pt growth on the NPG enhanced catalytic activity despite the smaller platinum loading.[3−5,17,44,45] In the case realized in this work, however, five SLRR events are expected to be sufficient in entirely covering the surface. Scanning Tunneling Microscopy demonstrated in our previous work[20] that the replacement event resulted in isolated islands of Pt that merged together in a continuous thin film after several (less than five) successive replacement steps.

4. Formic Acid Oxidation. The Pt coating described in the previous section is expected to minimize the CO poisoning of the catalyst early on in the formic acid oxidation because of the ultra low thickness and uneven morphology of the Pt deposit[20]

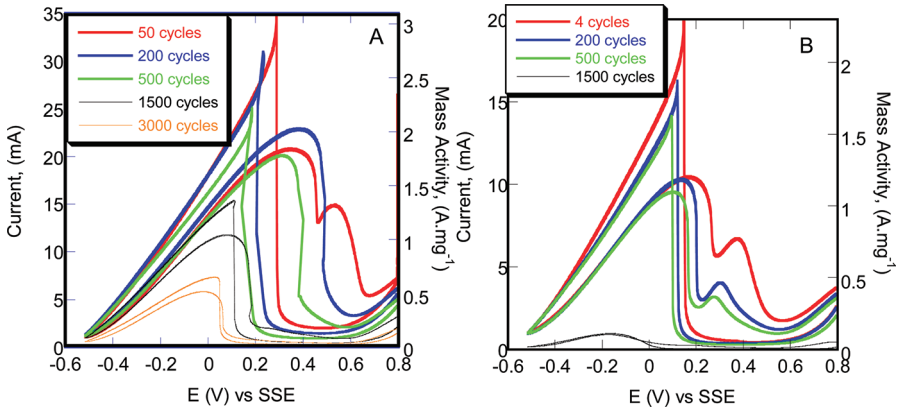

Figure 6. Formic acid oxidation on (a) 1:1 Ag:Au on Au and (b) 1:1 Ag:Au on GC. The CV curves are also normalized per unit mass of combined Pt−Au catalyst (right axis). Sweep rate −50 mV s^{-1}.

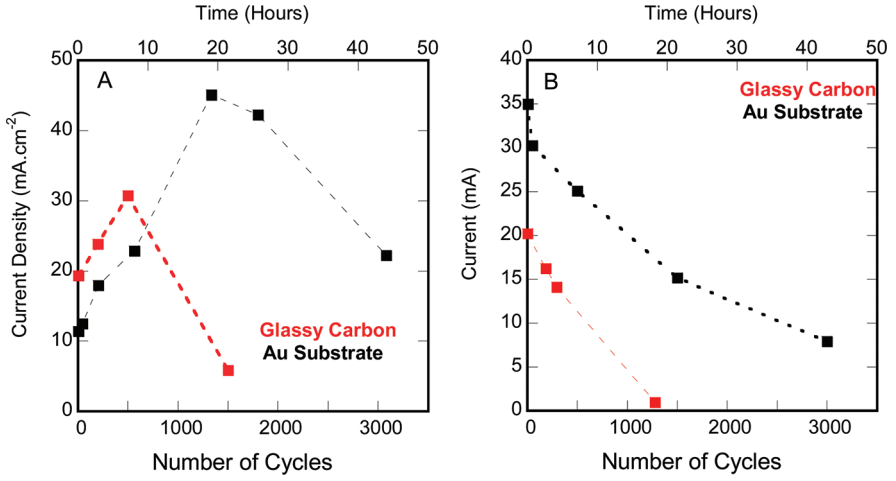

Figure 7. (A) Current density and (B) nominal current profiles of Pt-NPG catalysts from 1:1 Ag:Au deposit on Au substrate and GC substrate.

allowing for substrate impact on the catalytic behavior.[2] In this work, the formic acid oxidation tests on the alloys deposited on GC electrodes were considered initially to be more accurate in determining the activity of the Pt-NPG catalyst because those synthesized on Au would experience additional substrate contribution to the catalytic activity. GC provided an inert substrate so only the effects due to the grown Au functionalized by Pt were visible. The curves presented in Figure 6 illustrate the onset of passivity associated with CO adsorption on the electrode in the positive run to take place at approximately 0.400 V. Upon negative scanning, the passivity layer was broken apart, which generated a fresh surface prone to the formic acid oxidation process. This led to the substantial increase in current density at about 0.300 V on the Au substrate and about 0.150 V on the GC substrate.[33] The formic acid oxidation showed very high activity initially for the catalysts on both Au and GC, with current densities of more than 50 and 45 mA cm^{-2}, respectively. Also, presenting the data in mass activity (current per unit mass), Figure 6a and b - right axis, it is clear that the catalysts developed in this work feature peak mass activity values in the range 1−3 A mg^{-1}. This appears to be close to the higher performance end of recently developed catalysts for formic acid oxidation.[46,47] Along with performing slightly better initially, the catalyst on the Au substrate also demonstrated higher durability by withstanding over 2600 cycles. As the main focus of the present study was to examine the feasibility of an all-electrochemical approach for producing a Pt/NPG thin film catalyst for formic acid oxidation, this work is limited to a "proof-of-concept" level of studying this system. Apparently, further work is needed to precisely register and understand the trends in performance and optimize a variety of parameters on the as-developed catalyst.[3,34,35] It will be after this future study, when a comprehensive comparison with previously studied Pt nanoparticle catalysts described in the literature could be deemed accurate.

While general in nature, the results obtained herein are sufficient to reveal the significant difference in durability between the catalysts deposited on Au and the GC as substrates. More specifically, the catalyst deposited on the GC substrate appeared to be much less stable than the one on Au as evident by Figure 7a and b where the current density and nominal current are plotted as a function of the cycling time. As no substantial difference in the processes taking place on both catalysts should be anticipated, the loss of activity was most likely due to structural changes and physical loss of the catalyst deposited on GC. Due to the poor adhesion to the GC substrate, it was possible that a significant amount of the large-size spherical alloy particles had mechanically disconnected from the electrode in the course of formic acid oxidation testing. Indeed these effects could be

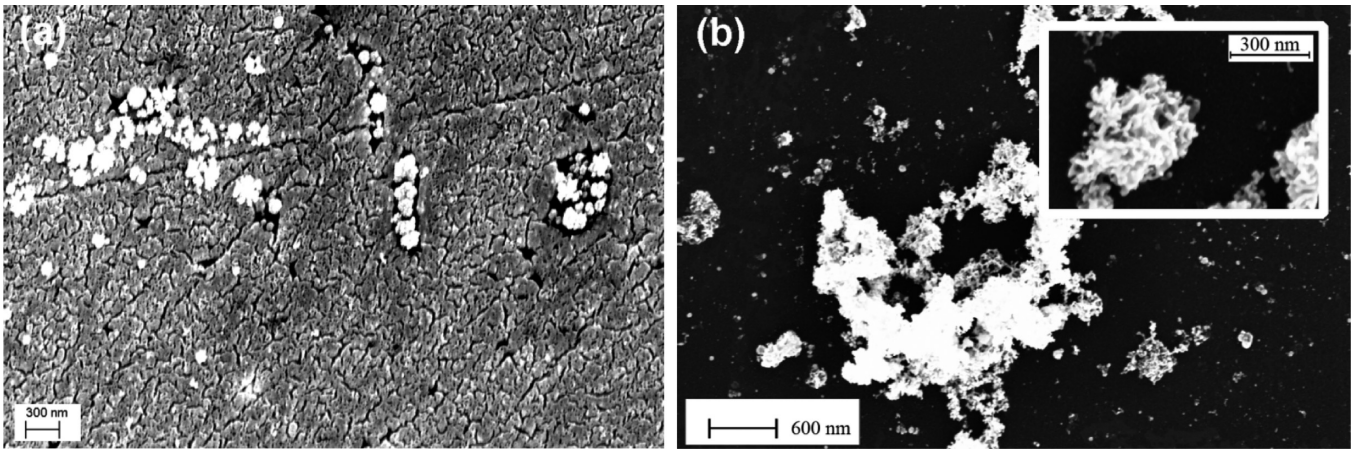

Figure 8. SEM images of the Pt-NPG catalyst on (a) Au and (b) GC after formic acid oxidation.

associated with mechanical interactions, such as the transfer of the electrode between solutions, rinsing with water and/or even gravitational effects. Also, the high current densities resulting in the growth of large CO/CO_2 bubbles typical for this type of testing[26] also contributed to the possibility of pulling particles off of the surface. Figure 8 displays SEM images of the catalyst following formic acid oxidation. The nanoporous structure was still present, indicating minimal coarsening of the surface. The H UPD curves in Figure 6, however, show a decrease in surface area and indicate a loss of electrochemical activity of the surface. Decay of catalytic activity is therefore mostly due to the general loss of Pt through dissolution routes,[48,49] poisoning of the surface by CO and, in the case of GC, additionally, to physical loss of particles that becomes obvious upon comparison of Figures 3e and 8b. Overall, in this work, the Pt-NPG film deposited on Au provides a better reference point for comparison of the as-developed catalyst to catalysts synthesized through other methods since it demonstrates without side effects the limits of achievable activity and durability. Apparently, substantial work needs to be done for the improvement of the adhesion of the GC catalyst so that a viable comparison could be made between Au and GC substrates as catalyst carriers.

CONCLUSIONS

The work reported on herein introduces and demonstrates in detail the steps of an all-electrochemical approach for synthesis of a Pt functionalized NPG catalyst for application in fuel cell catalysis and in particular, for formic acid oxidation. The synthetic route includes electrodeposition of $Au_{(1-x)}Ag_x$ alloy from a thiosulfate based solution containing Ag^+ ions and Au(I)Cl complex. Subsequent potential-controlled dealloying serves for the development of NPG thin film or spherical clusters deposited on Au or GC substrate, respectively. The dealloying of the thin films featured almost identical critical potentials with the bulk alloy counterparts while the spherical-particles shaped alloy was dealloying at more negative potentials likely owing to curvature effects. Once developed, the NPG is Pt-coated by five events of SLRR of Pb UPD layers. The surface area developed by dealloying and left unchanged after the Pt coating is comparable to the one that is generally obtained by same-size Pt nanoparticles catalyst. Tested in this work for activity and durability in the formic acid oxidation process, the as-developed catalysts demonstrated a remarkable initial activity in current density and mass activity based on peak current values (as high as 50 mA cm^{-2} and 1−3 A mg^{-1}, respectively) and durability of up to 2600 cycles. These benchmarking figures are generally comparable to those of best, same-size Pt and/or Pd nanoparticle catalysts.

This paper will be followed up by companion works where a thorough optimization effort will be made (i) on the activation of the GC substrate in order to enable stronger adhesion between more uniform and denser (nearly continuous) layers of Pt-NPG catalyst and (ii) on the improvement of the catalytic performance of the of pure Pt coating and introduction of bimetallic coatings instead by incorporation of other metals Pb, Cu, Pd, or Ru shown to significantly affect the rate of formic acid oxidation in the literature.

AUTHOR INFORMATION

Corresponding Author

*E-mail: dimitrov@binghamton.edu.

ACKNOWLEDGMENT

The authors of this work acknowledge the financial support of the National Science Foundation (DMR-CAREER-0742016).

REFERENCES

(1) Zhong, C. J.; Luo, J.; Fang, B.; Wanjala, B. N.; Njoki, P. N.; Loukrakpam, R.; Yin, J. *Nanotechnology* **2010**, *21* (6), 062001.

(2) Luo, J.; Maye, M. M.; Kariuki, N. N.; Wang, L.; Njoki, P.; Lin, Y.; Schadt, M.; Naslund, H. R.; Zhong, C.-J. *Catal. Today* **2005**, *99* (3−4), 291–297.

(3) Ding, Y.; Chen, M.; Erlebacher, J. *J. Am. Chem. Soc.* **2004**, *126* (22), 6876–6877.

(4) Zeis, R.; Mathur, A.; Fritz, G.; Lee, J.; Erlebacher, J. *J. Power Sources* **2007**, *165* (1), 65–72.

(5) Park, I.-S.; Lee, K.-S.; Choi, J.-H.; Park, H.-Y.; Sung, Y.-E. *J. Phys. Chem. C* **2007**, *111* (51), 19126–19133.

(6) Erlebacher, J.; Aziz, M. J.; Karma, A.; Dimitrov, N.; Sieradzki, K. *Nature* **2001**, *410* (6827), 450–453.

(7) Jia, F.; Yu, C.; Deng, K.; Zhang, L. *J. Phys. Chem. C* **2007**, *111* (24), 8424–8431.

(8) Angurel, L. A.; Amaveda, H.; Natividad, E.; Castro, M.; Andres, J. M.; Bona, M. T. *IEEE Trans. Appl. Supercond.* **2007**, *17* (2), 3012–3015.

(9) Mathur, A.; Erlebacher, J. *Surf. Sci.* **2008**, *602* (17), 2863–2875.

(10) Zhang, J.; Lima, F. H. B.; Shao, M. H.; Sasaki, K.; Wang, J. X.; Hanson, J.; Adzic, R. R. *J. Phys. Chem. B* **2005**, *109* (48), 22701–22704.
(11) Wittstock, A.; Neumann, B. r.; Schaefer, A.; Dumbuya, K.; Kübel, C.; Biener, M. M.; Zielasek, V.; Steinrück, H.-P.; Gottfried, J. M.; Biener, J. r.; Hamza, A.; Baümer, M. *J. Phys. Chem. C* **2009**, *113* (14), 5593–5600.
(12) Liu, Y.; Bliznakov, S.; Dimitrov, N. *J. Electrochem. Soc.* **2010**, *157* (8), K168–K176.
(13) Nagahara, Y.; Hara, M.; Yoshimoto, S.; Inukai, J.; Yau, S. L.; Itaya, K. *J Phys Chem B* **2004**, *108* (10), 3224–3230.
(14) Waibel, H. F.; Kleinert, M.; Kibler, L. A.; Kolb, D. M. *Electrochim. Acta* **2002**, *47* (9), 1461–1467.
(15) Ding, Y.; Chen, M. *MRS Bull.* **2011**, *34* (08), 569–576.
(16) Deng, Y.; Huang, W.; Chen, X.; Li, Z. *Electrochem. Commun.* **2008**, *10* (5), 810–813.
(17) Zhang, J.; Liu, P.; Ma, H.; Ding, Y. *J. Phys. Chem. C* **2007**, *111* (28), 10382–10388.
(18) Brankovic, S. R.; Wang, J. X.; Adzic, R. R. *Surf. Sci.* **2001**, *474* (1−3), L173–L179.
(19) Kim, Y. G.; Kim, J. Y.; Vairavapandian, D.; Stickney, J. L. *J Phys Chem B* **2006**, *110* (36), 17998–18006.
(20) Fayette, M.; Liu, Y.; Bertrand, D.; Nutariya, J.; Vasiljevic, N.; Dimitrov, N. *Langmuir* **2011**, *27* (9), 5650–5658.
(21) Vasilic, R.; Dimitrov, N. *Electrochem. Solid-State Lett.* **2005**, *8* (11), C173–C176.
(22) Ge, X.; Wang, R.; Liu, P.; Ding, Y. *Chem. Mater.* **2007**, *19* (24), 5827–5829.
(23) Kristian, N.; Yan, Y.; Wang, X. *Chem. Commun.* **2008**, *3*, 353–353.
(24) Wang, R.; Wang, C.; Cai, W.-B.; Ding, Y. *Adv. Mater.* **2010**, *22* (16), 1845–1848.
(25) Liu, Y.; Bliznakov, S.; Dimitrov, N. *J. Phys. Chem. C* **2009**, *113* (28), 12362–12372.
(26) Xu, D.; Bliznakov, S.; Liu, Z.; Fang, J.; Dimitrov, N. *Angew. Chem.* **2010**, *122* (7), 1304–1307.
(27) Green, T. A.; Liew, M. J.; Roy, S. *J. Electrochem. Soc.* **2003**, *150* (3), C104–C110.
(28) Liew, M. J.; Roy, S.; Scott, K. *Green Chem.* **2003**, *5* (4), 376.
(29) Osaka, T.; Kato, M.; Sato, J.; Yoshizawa, K.; Homma, T.; Okinaka, Y.; Yoshioka, O. *J. Electrochem. Soc.* **2001**, *148* (10), C659–C662.
(30) Osaka, T.; Kodera, A.; Misato, T.; Homma, T.; Okinaka, Y.; Yoshioka, O. *J. Electrochem. Soc.* **1997**, *144* (10), 3462–3469.
(31) Green, T. A.; Roy, S. *J. Electrochem. Soc.* **2006**, *153* (3), C157–C163.
(32) Okinaka, Y.; Hoshino, M. *Gold Bull.* **1998**, *31* (1), 3–13.
(33) Ivanov, S.; Tsakova, V. *Electrochim. Acta* **2005**, *50* (28), 5616–5623.
(34) Sieradzki, K.; Dimitrov, N.; Movrin, D.; McCall, C.; Vasiljevic, N.; Erlebacher, J. *J. Electrochem. Soc.* **2002**, *149* (8), B370–B377.
(35) Parida, S.; Kramer, D.; Volkert, C.; Rösner, H.; Erlebacher, J.; Weissmüller, J., *Phys. Rev. Lett.* 2006, *97* (3).
(36) Scaglione, F.; Gebert, A.; Battezzati, L. *Intermetallics* **2010**, *18* (12), 2338–2342.
(37) Lu, X.; Balk, T.; Spolenak, R.; Arzt, E. *Thin Solid Films* **2007**, *515* (18), 7122–7126.
(38) Dursun, A.; Pugh, D. V.; Corcoran, S. G. *Electrochem. Solid-State Lett.* **2003**, *6*, B32–B34.
(39) Dursun, A.; Pugh, D. V.; Corcoran, S. G. *J. Electrochem. Soc.* **2005**, *152*, B65–B72.
(40) Bonou, L.; Eyraud, M.; Crousier, J. *J. Appl. Electrochem.* **1994**, *24*, 906–10.
(41) Sieradzki, K.; Corderman, R. R.; Shukla, K.; Newman, R. C. *Philos Mag A* **1989**, *59* (4), 713–746.
(42) Li, R.; Sieradzki, K. *Phys. Rev. Lett.* **1992**, *68* (8), 1168–1171.
(43) Mayrhofer, K. J. J.; Strmcnik, D.; Blizanac, B. B.; Stamenkovic, V.; Arenz, M.; Markovic, N. M. *Electrochim. Acta* **2008**, *53* (7), 3181–3188.
(44) Zhang, J.; Sasaki, K.; Sutter, E.; Adzic, R. R. *Science* **2007**, *315* (5809), 220–222.
(45) Zhang, J.; Vukmirovic, M. B.; Sasaki, K.; Nilekar, A. U.; Mavrikakis, M.; Adzic, R. R. *J. Am. Chem. Soc.* **2005**, *127* (36), 12480–12481.
(46) Zhou, Z. Y.; Kang, X. W.; Song, Y.; Chen, S. W. *Chem. Commun.* **2011**, *47* (21), 6075–6077.
(47) Zhou, W. J.; Lee, J. Y. *Electrochem. Commun.* **2007**, *9* (7), 1725–1729.
(48) Ferreira, P. J.; la O', G. J.; Shao-Horn, Y.; Morgan, D.; Makharia, R.; Kocha, S.; Gasteiger, H. A. *J. Electrochem. Soc.* **2005**, *152* (11), A2256–A2271.
(49) Mayrhofer, K. J. J.; Meier, J. C.; Ashton, S. J.; Wiberg, G. K. H.; Kraus, F.; Hanzlik, M.; Arenz, M. *Electrochem. Commun.* **2008**, *10* (8), 1144–1147.